TuNR: Orthogonal Control of Mean and Variability of Endogenous Genes in a Human Cell Line

Alain R. Bonny[1,3], João Pedro Fonseca[1,3,4], Jesslyn E. Park[1], Hana El-Samad[1,2*]

[1]Department of Biochemistry and Biophysics, University of California, San Francisco, San Francisco, CA 94158

[2]Chan Zuckerberg Biohub, San Francisco, CA 94158

[3]Contributed Equally

[4]Present address: Amyris Bio Products Portugal, Porto, Portugal

*To whom correspondence should be addressed: Hana.El-Samad@ucsf.edu

Abstract

Stochastic fluctuations at the transcriptional level contribute to isogenic cell-to-cell heterogeneity in mammalian cell populations. However, we still have no clear understanding of the repercussions of this heterogeneity, given the lack of tools to independently control mean expression and variability of a gene. Here, we engineered a synthetic circuit to independently modulate mean expression and heterogeneity of transgenes and endogenous human genes.

The circuit, a Tunable Noise Rheostat (TuNR), consists of a transcriptional cascade of two inducible transcriptional activators, where the output mean and variance can be modulated by two orthogonal small molecule inputs. In this fashion, different combinations of the inputs can achieve the same mean but with different population variability. With TuNR, we achieve low basal expression, over 1000-fold expression of a transgene product, and up to 7-fold induction of the endogenous gene *NGFR*. Importantly, for the same mean expression level, we are able to establish varying degrees of heterogeneity in expression within an isogenic population, thereby decoupling gene expression noise from its mean. TuNR is therefore a modular tool that can be used in mammalian cells to enable direct interrogation of the implications of cell-to-cell variability.

Introduction

Clonal cells within a population can display tremendous variability in their physical characteristics (e.g. morphology), their molecular contents, as well as their transcriptional and signaling states, leading to distinct phenotypes and cell fate decisions in response to the same stimulus[1–6]. The roots of this cell-to-cell variability within a population are many, including distinct microenvironments or paracrine signaling[7]. However, a main driver of population heterogeneity is at the level of transcription[8,9,10]. While certain “housekeeping” genes (e.g. ribosome biogenesis) can display remarkably uniform expression between cells, other genes can exhibit widely heterogeneous expression[11]. Uncovering how transcriptional fluctuations differentially direct downstream network activities to cause divergent behaviors from the average of the population has been a long-standing research effort[12,13]. In unicellular organisms, cell-to-cell variability in gene expression has been shown to confer survival under extreme duress in a phenomenon known as bet-hedging[14,15]. Bet-hedging in microbial populations is one example

where variable transcriptional activity can drive phenotypic behaviors, which has been implicated in antibiotic resistance[16–18]. In multicellular organisms, transcriptional heterogeneity has been observed to at least partially influence cell fate decisions such as stem cell differentiation[13], the HIV latent-active decision[19], and drug resistance upon selection[20,21].

While numerous observations implicating gene expression heterogeneity in differential phenotypes have been documented, determining the causal effect of this variability can only be done when it is the only experimental variable that is changed in a study. This has proven to be challenging because genetic manipulations that change variability, for example through the suppression or over-expression of a gene, also change mean gene expression. Interrogating hypotheses about variability therefore awaits strategies that can deconvolve the effects of changes in the mean expression of a gene from its variability. A synthetic biology approach is uniquely suited to address this challenge[20,22–27], as shown through the use of optogenetic pulsing[28], negative and positive feedback[20], as well as titratable, independent production and degradation of a protein of interest[29,30,31]. While presenting valuable proofs of concepts, these strategies remain challenging to deploy for biological studies in mammalian systems. For example, the optogenetic pulsing strategy allows for the same circuit to overexpress and independently modulate gene variability in response to different inputs of blue light. However, this strategy has only been vetted for transgene regulation in *Saccharomyces cerevisiae,* with non-trivial barriers to implementation in mammalian systems. The strategy relying on the use of negative and positive feedback to regulate the mean and heterogeneity in gene expression requires different genetic circuits and cell lines in order to achieve similar means with different variances, representing a cell engineering challenge. Lastly, while controlling protein production independent of its degradation is an elegant implementation to modulate mean and variability, this circuit relies on inserting a transgene and appending a destabilizing domain to the protein of

interest, potentially perturbing its endogenous function. Additionally, modifying endogenous loci with the destabilization domain is not modular, nor does it allow for high-throughput testing of different genes. While each of the aforementioned studies has advanced our understanding, a strategy that is amenable to a wide range of mammalian expression systems, is modular to target transgene and endogenous loci, and can decouple changes in mean from variance, is still needed.

To address this challenge, we looked to an earlier synthetic circuit that utilized a serial orientation of independent inducible transcription factors to decouple mean expression from variability[32]. We engineered an analogous small molecule dual-inducible synthetic circuit in human cells, which we named a Tunable Noise Rheostat (TuNR), to independently titrate the mean expression and variability of transgene and endogenous gene products in a mammalian cell line (PC9). This cascading-activator circuit arrangement achieved approximately 1000-fold induction of transgene expression. Furthermore, different dosage regimes of the two small molecules could achieve the same mean gene expression (isomeans) with different variability within a population. As a proof of concept, we deployed TuNR to the endogenous loci of genes *NGFR* and *CXCR4*. Used in this endogenous context, the circuit can induce expression up to 7.2-fold for *NGFR* and 3.4-fold for *CXCR4*. In both cases, however, we could achieve isomean combinations of inducers where TuNR can modulate the variability of *NGFR* and *CXCR4* expression independent of their means. These data position TuNR as a modular circuit that allows protein mean expression and variability control, enabling systematic explorations of the specific consequences of mean expression of a gene versus its variability in mammalian cells.

Results

Construction and validation of a serial circuit topology consisting of two inducible transcriptional activation systems

We built TuNR as a serial connection of two inducible transcriptional activation systems, where the upstream system (first node) controls production of the downstream system (second node) (Figure 1A, Supplemental Figure 1A). The first node consists of a Gal4 DNA binding domain fused to half of a split abscisic acid (ABA) binding domain that, in the presence of ABA, assembles with its cognate heterodimer fused to a VP-16 activation domain[33,34]. The recruitment of the ABA-reconstituted gene product of the first node to the Upstream Activating Sequence minimal promoter (pUAS) drives the expression of the second inducible system and mRuby as a reporter. This second node consists of a *Staphylococcus Pyogenes* nuclease-dead Cas9 (dCas9) N-terminally fused to half of a gibberellic acid (GA) binding domain and a VPR (p65, VP65, Rta) activation domain appended to the other half of the GA binding domain. In the presence of GA, these two proteins dimerize, and upon the concomitant expression of a target guide RNA (gRNA), are able to induce expression of the gene of interest (Figure 1A). We identified ABA and GA as small molecule inducers of choice due to their low impact on mammalian physiology, reversibility of cognate protein dimerization, and the orthogonality of each heterodimerization event[34,35,33]. Moreover, we chose dCas9 as the final node of TuNR for its modularity in targeting any locus with an appropriate protospacer adjacent motif.

We integrated TuNR together with a gRNA cassette targeting the Tetracycline Response Element (pTRE) and a pTRE-driven mAzamiGreen reporter in PC9 cells (Figure 1A). In order to limit confounding effects of random integration of the circuit, we isolated and propagated cell lines from single cell clones. To characterize the steady-state expression of the first node of the circuit, we induced expression with varying concentrations of ABA and measured mRuby expression daily over 7 days, replenishing the induction media every 24 hours. We observed

graded mRuby activation at all doses with each reaching steady state by day 3 and maintaining their respective mRuby expression for the remainder of the experiment (Figure 1B, Supplementary Figure 1B). Next, we characterized expression of the second node in a separate experiment by maximally priming cells with 400 μM ABA for 3 days and then titrating the amount of GA. Similar to the first node characterization, we measured mAzamiGreen expression and replenished media every 24 hours over 7 days. As expected, we observed proportional induction of the second inducible node, as mAzamiGreen levels reached steady state by day 6 for all dosages (Figure 1C). In each of these experiments, we observed an approximately 100-fold induction for each respective node, consistent with previous reports[33]. Cells that were not exposed to either ABA or GA had nearly 10-fold lower mAzamiGreen expression than ABA-primed cells due to the lack of basal dimerization from the split GA recruitment domains (Supplementary Figure 1C). Importantly, induction of TuNR with ABA and GA showed that mRuby expression, which reports on the activity of the first node, responds uniquely to ABA, and not to GA, confirming that these two small molecules have little cross-reactivity (Supplemental Figure 1D).

To explore a more comprehensive range of expression for mAzamiGreen in response to simultaneous ABA and GA induction, we primed the cells with a dose response of ABA for 3 days and, while continuing ABA induction, titrated induction with GA and measured the expression of mAzamiGreen (Figure 1D). As expected, the absence of both ABA and GA (top left corner) set the basal expression of mAzamiGreen with the lowest amount possible from TuNR. As an illustration of the benefit of the cascade transcriptional activator arrangement, without ABA, we detected little change in terminal node activation in response to increasing GA (top row, Figure 1D). Conversely, in the absence of GA, TuNR displays 6-fold induction upon addition of ABA, consistent with earlier experiments suggesting that leakiness emerges from the

accumulation of the first node activator (first column, Figure 1D). When both small molecules are present, TuNR induces expression more than either small molecule alone, reaching a maximum mAzamiGreen expression of approximately 1000-fold when both inducers are at their highest concentration. Notably, a transcriptional activator circuit mediated by GA (rows of Figure 1D), achieves approximately 100-fold induction. As the concentration of ABA increases, so does the basal expression. This reflects a tradeoff between maximum expression and basal leakiness (Figure 1D, E). The serial arrangement of the transcriptional activators attenuates this basal leakiness, while achieving a superior maximum fold-change induction when compared to a single-node circuit.

Inducible gene expression systems both in microorganisms[36,37,38] and mammalian cells[34,35,39,40] have historically suffered from leaky basal expression in the absence of inducer. Our data indicate that the serial topology of TuNR, through the combination of chemically-inducible orthogonal recruitment domains, was able to generate a two-input and one-output system with low basal activity with a smooth continuum of expression values. Intuitively, the cascade structure is acting as a coincidence detector in which the output relies on the unlikely simultaneous activation of two transcriptional activators under basal conditions (no small molecule inputs), therefore mediating a low basal activity. However, upon induction with both small molecule activators, output expression is enabled, and can be precisely controlled by titrating both independent inputs. We next set out to investigate whether cell-to-cell variability might also be modulated in this circuit topology through different combinations of the small molecule inputs.

Serial topology of TuNR enables independent control of transgene mean expression and noise

The topology of the TuNR circuit has been shown to allow for the independent control of the mean and variance of the expression of transgenes in yeast[29,32]. To explore the ability of TuNR to control population heterogeneity in the expression of a transgene of interest in mammalian cells, we generated a clonal PC9 cell line that has two identical pTRE promoters that are targeted by the second node and independently drive the expression of both mAzamiGreen and tagBFP (Figure 2A). We induced TuNR with a two-dimensional dose-response of ABA and GA as previously described, and measured mAzamiGreen and tagBFP expression at steady state. Induction of TuNR with ABA and GA showed similar effects on the mean expression of mAzamiGreen and tagBFP, with both fluorescent proteins displaying correlated, increasing expression with both inducers (Supplementary Figure 2).

In order to quantify the total noise for every combination of ABA and GA, we utilized a common noise decomposition strategy to ascertain the extrinsic and intrinsic contributions to the expression noise as shown previously[8]. In this analysis, the correlated expression between the two terminal fluorophores represents the extrinsic noise, or cell-to-cell variability; whereas the uncorrelated expression is the intrinsic noise, or the cumulative intracellular stochastic effects (Figure 2B, Supplementary Figure 3)[41]. Based on prior studies, we hypothesized that due to the serial topology of TuNR, different combinations of ABA and GA could achieve the same mean expression, but with different extrinsic noise values. To quantify the noise in the system we used the coefficient of variation (CV^2). Consistent with the notion that stochastic effects due to counting noise diminish with increasing mean, we observed a strong anti-correlated relationship between intrinsic noise and mean expression (Figure 2C). Contrary to the intrinsic noise trend, we observed that extrinsic noise was less dependent on increasing mean, where different combinations of ABA and GA achieved the same mean with different extrinsic noise values (Figure 2C). We further investigated these “isomean” distributions, and a common pattern

emerged: cells exposed to the lower amount of ABA and higher amount of GA had wider histogram distributions, suggestive of more cell-to-cell variability, than cells exposed to high amounts of ABA and lower of GA (Figure 2D, Supplemental Figure 4). The multiplier effect between serially-arranged transcriptional activators, which has been previously demonstrated to achieve noise modulation, maintains its efficacy in this more complex eukaryotic system[10,32]. This observation was consistent across both terminal fluorophores, and another clonal cell line of the circuit that likely has a different number of circuit integrations, suggesting that the circuit topology of TuNR is driving this behavior (Supplemental Figure 5). To visualize the heterogeneity, we imaged the mRuby and mAzamiGreen expression in two representative isomean wells (Figure 2E). Images of these cells further reinforce that a high concentration of ABA (high expression of mRuby) combined with low concentration of GA gives rise to a tighter distribution that displays a more uniform, average mAzamiGreen expression among cells. Conversely, a lower concentration of ABA (low expression of mRuby) with higher amounts of GA lead to wider distributions and the presence of both low- and high-expressing mAzamiGreen cells (Figure 2E). These data establish TuNR as a synthetic circuit that can be deployed to decouple mean expression and the extrinsic noise of a transgene of interest.

TuNR enables independent control of population mean and variance of endogenous genes

Given the capabilities of dCas9, we next attempted to challenge TuNR by testing its efficacy and modularity against endogenous loci. We chose the genes *NGFR* and *CXCR4* for the first proof of concept because their encoded proteins are both membrane-bound, and could be stained at the surface of live cells with commercial antibodies. Additionally, *NGFR* and *CXCR4* have been previously implicated as proliferative and metastatic oncogenes,

respectively[21,42]. These two genes represent distinct expression paradigms to assess independent mean and variability control: *NGFR*, which is not expressed in PC9 cells[21]; and *CXCR4*, which is constitutively transcribed by the parental cell line[43]. By targeting *NGFR*, we sought to test the extent of control in a gene absent active transcriptional machinery at its locus. In the case of *CXCR4*, due to its native constitutive expression, TuNR would compete with endogenous transcriptional and translational machinery in regulating protein abundance.

To target the circuit to endogenous loci in a modular fashion, we built a modified TuNR "chassis" clonal cell line without a gRNA cassette, and confirmed that the first node of the circuit reached steady state with comparable kinetics to the original TuNR (Supplementary Figure 6A, B). We transduced the cells with lentivirus carrying previously-vetted gRNAs that target either the *NGFR* (Figure 3A) or *CXCR4* (Figure 3B) promoters with a tagBFP reporter indicative of integration[44]. We then induced cells with ABA and GA at varying concentrations, reproducing the two-dimensional dose response matrix described earlier, and measured protein levels of *NGFR* and *CXCR4* (Supplemental Figure 6C, D).

TuNR achieved 7.2-fold mean induction for *NGFR* and 3.4-fold induction for *CXCR4* and (Figure 3C, D), which are levels comparable to what other systems have achieved with CRISPRa[45,46]. Additionally, as observed in modulating mAzamiGreen, TuNR showed a negligible effect on basal levels of *NGFR* and *CXCR4* (Figure 3C, D), demonstrating that TuNR minimally perturbs basal gene expression due to its serial topology .

Furthermore, distributions of protein abundance at different levels of ABA and GA induction showed a nearly three- and two-fold range of tunable extrinsic noise for *NGFR* and *CXCR4*, respectively (Figure 3E, F). Here again, when comparing distributions with the same mean for both *NGFR* (Figure 3G, I) and *CXCR4* (Figure 3H, J) we found that low ABA and high GA gave rise to wider distributions, while high ABA and low GA reproducibly gave rise to

narrower distributions of expression in the cell populations (Supplementary Figure 7). These results illustrate that TuNR is able to precisely and orthogonally control select genes from their endogenous loci and produce cellular populations with distinct means and variances in a manner consistent with transgene regulation.

Discussion

Advances in synthetic biology have enabled novel investigations into fundamental aspects of biology and ushered in a sea change in biotechnology and bioengineering. The main driver of this paradigm shift is the development of new and more precise tools that are modular, robust, and open new lines of questioning. Despite enhancements in the suite of tools available for mammalian gene regulation, the ability to finely control the mean and variability of gene expression has long-been outstanding, and previous efforts in mammalian expression systems have often convolved these two parameters. To address this need, we developed TuNR, which acts as a versatile and modular tool to effectively decouple control of the mean from the variance in gene expression. To accomplish this, we arranged two orthogonal, inducible expression systems serially so that by tuning the concentrations of each respective inducer, we can achieve combinations with the same mean expression, yet different extrinsic noise properties for targeted genes of interest. From this topology, we demonstrated a dynamic range of nearly 1000-fold inducible transgene expression while reducing basal leakiness 10-fold when compared to a single-node circuit. In addition to this precise control over the mean, this circuit topology enables independent control over the population variability. With the inherent versatility of CRISPR technology, developing a chassis TuNR allows multiple genes to be investigated in parallel. To that end, the precise control of gene expression mean and variability was not limited to transgenes, and extended to endogenous loci.

We believe the main contribution of TuNR is in its ability to be a multifaceted tool towards precise gene regulation. While the induction capabilities of TuNR and other comparable CRISPRa-based systems in activating endogenous gene expression is modest relative to transgenes, we argue that precisely regulating the distribution of gene expression will be of tremendous value in future investigations. It is likely that our ability to achieve small fold changes for endogenous genes compared to transgene is related to a lack of clear understanding of enhancer-promoter mechanisms and corrective cellular mechanisms that counteract the action of the synthetic circuit. Understanding these effects will enable synthetic circuits to more robustly drive endogenous gene production. However, as much has been learned upon the adoption of titratable expression systems versus unregulated overexpression, we anticipate that granular control over the shape of a gene expression distribution will make similar contributions to the field. Furthermore, since it is well established that genes rarely operate in isolation, by modifying the gRNA cassette, one can conceivably multiplex target modulation in the same controlled manner. By establishing the TuNR cascade topology as a tractable and versatile system in mammalian cells, it would be interesting to attach different effector domains to the second node to further probe the effects of noisy gene perturbations, not limited to CRISPRa.

The work presented here opens new avenues to precisely interrogate one of the most fundamental aspects of biological systems: cell-to-cell variability. TuNR is a powerful new tool that will enable genetic perturbations with precise control, and thus allow for future studies to answer expression variability- and magnitude-dependent questions.

Main Figure Captions

Figure 1: **TuNR reduces basal leakiness, amplifies fold change, and expands accessible dynamic range relative to single inducible activator for transgene expression.** a) Diagram of TuNR circuit composed of a constitutively expressed Abscisic Acid (ABA)-inducible split system consisting of Gal4 and VP16. This inducible system drives the expression of mRuby as a reporter and a Gibberellic Acid (GA)-induced split system consisting of dCas9 and VPR. Addition of GA and constitutive expression of the guide RNA (gRNA, not pictured) targeted to the Tetracycline Responsive Element (pTRE) drives mAzamiGreen expression. b) Expression of mRuby from TuNR induced with increasing concentrations of ABA over 7 days. Media was replenished every 24 hours. c) Time-dependent mAzamiGreen expression. Cells were first induced with 400 μM of ABA for 3 days, at which increasing concentrations of GA were added. Measurements were carried out over the following 7 days while keeping ABA and GA concentration constant through daily replenishment. d) Heatmap of steady-state mAzamiGreen expression upon varying ABA induction (y-axis) and GA induction (x-axis). Data were collected on Day 6 after addition of ABA, and on Day 3 after addition of GA. e) Quantification of mAzamiGreen at steady state as a function of GA (x-axis) and ABA (shades of red). Error bars represent the Standard Error (SE) of n=2 independent replicates.

Figure 2: **TuNR confers independent control of population mean and variance in transgene expression.** a) Simplified diagram of TuNR shown in Figure 1A, with the addition of pTRE driving expression of tagBFP in the same cell to decompose intrinsic and extrinsic noise. b) Example of scatter plot of tagBFP and mAzamiGreen expression from TuNR induced with 4.94 μM ABA and 0 μM GA . Decomposition identifies two major axes of variance: intrinsic variance, which is the spread of points perpendicular to the diagonal; and extrinsic variance, represented by the spread of points along the diagonal. c) Plot of intrinsic (red), extrinsic (blue)

and total (green) noise, quantified using the coefficient of variation or CV^2, versus mean expression of mAzamiGreen of TuNR-containing cells exposed to different combinations of ABA and GA. d) Representative distributions of mAzamiGreen expression for different combinations of inducer molecules, as identified in Panel C (i, ii, iii, and iv), that achieve the same mean expression from one of two independent experiments. e) Images of mRuby expression and pseudo-colored mAzamiGreen expression corresponding to cells from the populations shown in Panel D, isomean IV.

Figure 3: **TuNR enables orthogonal control of population mean and variance of endogenous genes.** a) Simplified diagram of TuNR, as shown in Figure 1A, driving the expression of *NGFR* and b) *CXCR4* from their endogenous loci. c) Distributions of *NGFR* expression for no induction (orange) and max induction (purple) of TuNR. Also shown is the *NGFR* distribution in the parental cell line (green). d) Distributions of *CXCR4* expression for no induction (orange) and full induction (purple) of TuNR. Also shown is the *CXCR4* distribution in the parental cell line (green). e) Coefficient of variation of endogenous *NGFR*, as a function of mean expression, following the activation of TuNR for 6 days. f) Coefficient of variation of endogenous *CXCR4* as a function of its mean expression, following the activation of the TuNR for 6 days. g, i) Representative distributions of *NGFR* for different TuNR induction levels that achieve the same mean (isomean) but different variability as identified by grey strips in Panel E. h, j) Representative distributions of *CXCR4* for different TuNR induction levels that achieve the same mean (isomean) but different expression variability, as identified by grey strips in Panel F.

Supplemental Figure Captions

Supplementary Figure 1: **TuNR nodes are orthogonal and circuit has low basal expression of terminal output.** a) Full circuit diagram of TuNR targeted towards a pTRE promoter driving mAzamiGreen expression. b) Distributions of mRuby expression on day 3 with increasing doses of ABA (shades of red). Data are taken at day 3 when the means have reached steady-state (Figure 1B in the main text). c) Distributions of the expression of mAzamiGreen representing the abundance of dCas9 with (red) and without (beige) full induction of ABA. d) mRuby expression plotted as a function of ABA concentration with increasing amounts of GA (concentration increasing with shade of green). These are the same data as shown in Figure 1E in the main text. Error bars represent the SE of n=2 independent replicates.

Supplementary Figure 2: **First node of TuNR is responsive only to ABA, and second node is responsive to both ABA and GA.** a) Heatmap of steady-state mRuby expression in response to the activation of the first node of TuNR with increasing ABA concentration (y-axis), and increasing GA (x-axis). b) Heatmaps of steady-state mAzamiGreen (left) and tagBFP (right) expression with increasing ABA (y-axis), and increasing GA (x-axis).

Supplementary Figure 3: **Correlated expression of terminal outputs mAzamiGreen and tagBFP across 96 combinations of ABA and GA.** a) Representative scatter plots of tagBFP and mAzamiGreen expression from TuNR induced with 96 combinations of ABA and GA.

Supplementary Figure 4: **TuNR achieves several isomean combinations of inducers with different variability.** a) Heatmap of mean and b) CV^2 of mAzamiGreen expression. c) Example mAzamiGreen distributions binned by the same mean expression. d) Heatmap of mean and e)

CV^2 of tagBFP expression. f) Example tagBFP distributions binned by the same mean expression.

Supplementary Figure 5: **Mean expression and CV^2 from terminal nodes mAzamiGreen and tagBFP are strongly correlated across independent replicates and independent clones.** a) All-by-all plot of mean expression by well between mAzamiGreen and tagBFP, and across independent replicates and different clones of TuNR. R, Pearson Correlation Coefficient. b) All-by-all plot of well CV^2 between mAzamiGreen and tagBFP, and across independent replicates and different clones of TuNR.

Supplementary Figure 6: **TuNR "chassis" clonal cell lines reach steady state with comparable on-kinetics to previous TuNR cell lines.** a) Time-dependent mRuby expression of three independent clones, E11 (left), F5 (center), F11 (right) induced with increasing concentrations of ABA (shades of red). Error bars represent the 95% Confidence Interval of the mean. b) Clone F11 distributions of mRuby expression at steady-state (after 3 days) per dosage of ABA (shades of red). c) Heatmap of the mean expression of *NGFR* and d) *CXCR4* in the clone F11 background.

Supplementary Figure 7: **Trends of TuNR-mediated mean and variability control are maintained across independent replicates.** a) Plot of the 96 combinations of ABA and GA population mean expression of *NGFR* and b) *CXCR4* between independent replicates. R, Pearson Correlation Coefficient. c) Plot of the corresponding CV^2 for the same 96 combinations of ABA and GA for *NGFR* and d) *CXCR4* independent replicates.

Materials and Methods

Plasmid Construction

Plasmids were constructed using a hierarchical DNA assembly method as described previously[47,48]. All proteins had internal BsaI and BsmBI restriction sites removed prior to cloning. Proteins were introduced into the cloning system either by PCR or gene block (IDT), and were then assembled into transcriptional units. Transcriptional units were then assembled into final mutli-transcriptional unit (multi-TU) destination vectors to facilitate delivery to cells as described in the main text. To increase efficiency of integration, TuNR construct was split into two plasmids encoding full circuit. A third plasmid encoded pTRE driving mAzamiGreen and tagBFP, along with a mu6 cassette expressing a gRNA targeted to the pTRE promoter. All plasmids and cell lines will be available at Addgene, or upon request to the corresponding author.

Bacterial Cell Culture

Commercial MachI and XL10 strains (QB3 MacroLab) were used to transform plasmid vectors. A typical transformation mixture consists of 2 µL of the Golden Gate reaction product, 48 µL bacteria, incubated on ice for 30 minutes, heat shocked at 42 °C for 1 minute, recovered on ice for 5 minutes, reaction mixture plated onto selective agar and incubated overnight at 37 °C. In the case of multi-TU transformations, cells recovered in LB media for 30 min after heat shock at 37°C before plating reaction onto kanamycin selective agar plates. Cells were cultured in antibiotic concentrations of 100 µg/mL chloramphenicol (part domestication), 25 µg/mL carbenicillin (transcriptional unit) and 100 µg/mL kanamycin (multi-TU).

Mammalian Cell Culture

PC9 cells were maintained in RPMI media (Thermo) supplemented with 10% fetal bovine serum (UCSF Cell Culture Facility), 1% Glutamine (Gibco) and 1% Anti-Anti (Gibco). Cells were passaged every other day and maintained at 37 °C with 5% CO_2. For flow cytometry, cells were seeded at 1,500 cells/well in a 96-well flat-bottom plate (Corning) and allowed to adhere overnight. Cells were induced with ABA, and fresh media with ABA drug was replenished every 24 hours for 3 days. After 72 hours of ABA induction upon which steady-state has been reached, cells were induced with ABA and GA for 3 additional days.

Cell Line Generation

Cell lines used in Figures 1 and 2 were generated by co-transfecting parts one, two and three of the TuNR circuit in equimolar amounts in addition to PiggyBac Transposase (pCMV-hyPBase) using Lipofectamine 3000 (Thermo) according to manufacturer's instructions. TuNR "chassis" cell lines were generated as described above except by omitting part 3. All cell lines were clonally expanded from a single cell and verified to express circuit components by fluorophore proxy.

Lentiviral Production

Lentivirus particles were generated as described previously[47]. In short, LX-HEK293T cells were seeded at approximately 50% confluency in a 6-well plate, and the following day were transfected with lentiviral vector of interest alongside packaging plasmids (pCMV-dR8.91 and pCMV-VSV-G) using Lipofectamine 3000 (Thermo) according to manufacturer's instructions. After 72 hours, the supernatant was filtered through a 0.45 µm filter and added to PC9 cells in standard growth media supplemented with 4 µg/mL of polybrene (SCBT sc-134220) and centrifuged at 800 x g for 30 minutes. After 24 hours, media was exchanged for fresh media and assessed for selective marker expression after 72 hours.

Flow Cytometry

Flow cytometry was performed using a LSR Fortessa (BD) with a four laser configuration (488 nm, 635 nm, 355 nm, 405 nm). mAzamiGreen (excitation at 488 nm, emission at 530 nm), mRuby (excitation at 561 nm, emission between 610 and 620 nm), tagBFP (excitation at 355 nm, emission at 450 nm) and iRFP713 (excitation at 690 nm, emission at 713 nm) fluorescence levels were recorded for at least 10,000 events. To isolate single cell clones, cultures were fully induced with ABA and GA and single cells were isolated using a FACS Aria II (BD) into a 96-well flat-bottom plate based upon iRFP713, mRuby, and mAzamiGreen expression. Clonal cells were again screened for fluorescence activation after three weeks. For all experiments, cells were gated based on iRFP713 expression (presence of circuit).

Microscopy

Images were collected on a Nikon Ti Inverted Widefield Epifluorescence microscope with a mercury lamp to illuminate mAzamiGreen (excitation at 488 nm, emission at 530 nm) and mRuby (excitation at 561 nm, emission between 610 and 620 nm). Imaging was performed in a temperature and atmosphere controlled chamber collected through a 10x air objective with a 200 ms exposure time. Image histograms were normalized and pseudo-colored in Fiji (ImageJ).

Drug Compounds

Abscisic Acid (Sigma) and Gibberellic Acid (Santa Cruz Biotechnology) were prepared as individual 4000x stocks (1.6 M and 20 mM, respectively) and used to generate 96-well plates of mixed stock plates described below.

Drug stock preparation

Using an automated liquid handler (Labcyte Echo), drug stocks were prepared as 96-well plates (BioRad) at stock concentrations used for replicate experiments. Stock volumes were held constant with DMSO, and plates were stored at -20 °C.

Immunostaining

Cells were dissociated non-enzymatically using Versene Solution (Gibco™) at 37 °C for 20 min. The cells were then quenched in media and resuspended with wash buffer (10% FBS in DPBS) and transferred to a V-bottom 96-well plate. The cells were pelleted by centrifugation at 400 xg for 4 min. The plate was rapidly decanted and resuspended with 50 µL of corresponding antibody (1:400 in wash buffer) and incubated at room temperature in the dark for 1 hour. The cells were then washed with 100 µL of wash buffer and resuspended in 100 µL of wash buffer for immediate analysis by flow cytometry. Antibodies were purchased from ThermoFisher (CXCR4: #53-9991-80; NGFR: #PA5-20162). CXCR4 antibody and isotype were used at 1.25 µg/mL, and NGFR antibody and isotype were used at 1.25 µg/mL.

Data Processing and Statistical Analysis

Statistical and data analysis was executed using custom-written Python scripts.

Data Availability

All source data and code is available at https://github.com/arb5134/Rheostat.

Competing Interests

The authors declare no competing interests.

Author Contributions

A.R.B., J.P.F., H.E-.S. conceived of the study. A.R.B., J.P.F., J.E.P. designed and performed all experiments, and collected data. All authors interpreted the results and wrote the manuscript.

Acknowledgements

The authors thank members of the El-Samad lab for helpful guidance, feedback and discussion. The authors also thank Jason Town (UCSF), Ricardo Almeida (UCSF), Xiaoxiao (Vany) Sun (UCSF), Qiu Chang Wu (Harvard) and Zoë Steier (UC Berkeley) for early assistance and discussions. We thank the Steven Altschuler and Lani Wu labs for the gift of parental PC9 cells and the Wendell Lim lab for LX-HEK293T cells. H.E-.S is an investigator in the Chan Zuckerberg Biohub and this work was supported by the CZ-Biohub gift. This work was also supported by the National Science Foundation grant DBI-1548297 and National Science Foundation through grant NSF-MCB 1715108 awarded to H.E-.S, and the National Defense Science & Engineering Graduate (NDSEG) Fellowship awarded to A.R.B.

References

1. Charlebois, D. A., Abdennur, N. & Kaern, M. Gene expression noise facilitates adaptation and drug resistance independently of mutation. *Phys. Rev. Lett.* **107**, 218101 (2011).
2. Beaumont, H. J. E., Gallie, J., Kost, C., Ferguson, G. C. & Rainey, P. B. Experimental evolution of bet hedging. *Nature* **462**, 90–93 (2009).
3. Chang, A. Y. & Marshall, W. F. Dynamics of living cells in a cytomorphological state space. doi:10.1101/549246.
4. Spencer, S. L., Gaudet, S., Albeck, J. G., Burke, J. M. & Sorger, P. K. Non-genetic origins of cell-to-cell variability in TRAIL-induced apoptosis. *Nature* **459**, 428–432 (2009).
5. Weinberger, L. S., Burnett, J. C., Toettcher, J. E., Arkin, A. P. & Schaffer, D. V. Stochastic Gene Expression in a Lentiviral Positive-Feedback Loop: HIV-1 Tat Fluctuations Drive Phenotypic Diversity. *Cell* vol. 122 169–182 (2005).

6. Huh, D. & Paulsson, J. Random partitioning of molecules at cell division. *Proc. Natl. Acad. Sci. U. S. A.* **108**, 15004–15009 (2011).

7. Handly, L. N., Pilko, A. & Wollman, R. Paracrine communication maximizes cellular response fidelity in wound signaling. *Elife* **4**, e09652 (2015).

8. Elowitz, M. B., Levine, A. J., Siggia, E. D. & Swain, P. S. Stochastic gene expression in a single cell. *Science* **297**, 1183–1186 (2002).

9. Ebadi, H. *et al.* Patterning the insect eye: From stochastic to deterministic mechanisms. *PLoS Comput. Biol.* **14**, e1006363 (2018).

10. Blake, W. J., KÆrn, M., Cantor, C. R. & Collins, J. J. Noise in eukaryotic gene expression. *Nature* vol. 422 633–637 (2003).

11. Eisenberg, E. & Levanon, E. Y. Human housekeeping genes, revisited. *Trends Genet.* **29**, 569–574 (2013).

12. Balaban, N. Q., Merrin, J., Chait, R., Kowalik, L. & Leibler, S. Bacterial persistence as a phenotypic switch. *Science* **305**, 1622–1625 (2004).

13. Chang, H. H., Hemberg, M., Barahona, M., Ingber, D. E. & Huang, S. Transcriptome-wide noise controls lineage choice in mammalian progenitor cells. *Nature* **453**, 544–547 (2008).

14. Carey, J. N. *et al.* Regulated Stochasticity in a Bacterial Signaling Network Permits Tolerance to a Rapid Environmental Change. *Cell* **175**, 1989–1990 (2018).

15. Zhang, Z., Qian, W. & Zhang, J. Positive selection for elevated gene expression noise in yeast. *Mol. Syst. Biol.* **5**, 299 (2009).

16. Schmiedel, J. M., Carey, L. B. & Lehner, B. Empirical mean-noise fitness landscapes reveal the fitness impact of gene expression noise. *Nature Communications* vol. 10 (2019).

17. Blake, W. J. *et al.* Phenotypic consequences of promoter-mediated transcriptional noise. *Mol. Cell* **24**, 853–865 (2006).

18. Lehner, B. Selection to minimise noise in living systems and its implications for the evolution of gene expression. *Mol. Syst. Biol.* **4**, 170 (2008).

19. Dar, R. D., Hosmane, N. N., Arkin, M. R., Siliciano, R. F. & Weinberger, L. S. Screening for noise in gene expression identifies drug synergies. *Science* **344**, 1392–1396 (2014).

20. Farquhar, K. S. *et al.* Role of network-mediated stochasticity in mammalian drug resistance. *Nat. Commun.* **10**, 2766 (2019).

21. Shaffer, S. M. *et al.* Rare cell variability and drug-induced reprogramming as a mode of cancer drug resistance. *Nature* **546**, 431–435 (2017).

22. Murphy, K. F., Adams, R. M., Wang, X., Balázsi, G. & Collins, J. J. Tuning and controlling gene expression noise in synthetic gene networks. *Nucleic Acids Res.* **38**, 2712–2726 (2010).

23. Nevozhay, D., Adams, R. M., Murphy, K. F., Josic, K. & Balázsi, G. Negative autoregulation linearizes the dose-response and suppresses the heterogeneity of gene expression. *Proc. Natl. Acad. Sci. U. S. A.* **106**, 5123–5128 (2009).

24. Gao, X. J., Chong, L. S., Kim, M. S. & Elowitz, M. B. Programmable protein circuits in living cells. *Science* **361**, 1252–1258 (2018).

25. Roybal, K. T. *et al.* Engineering T Cells with Customized Therapeutic Response Programs Using Synthetic Notch Receptors. *Cell* **167**, 419–432.e16 (2016).

26. Morsut, L. *et al.* Engineering Customized Cell Sensing and Response Behaviors Using Synthetic Notch Receptors. *Cell* **164**, 780–791 (2016).

27. Guinn, M. T. & Balázsi, G. Noise-reducing optogenetic negative-feedback gene circuits in human cells. *Nucleic Acids Res.* (2019) doi:10.1093/nar/gkz556.

28. Benzinger, D. & Khammash, M. Pulsatile inputs achieve tunable attenuation of gene expression variability and graded multi-gene regulation. *Nat. Commun.* **9**, 3521 (2018).

29. Mundt, M., Anders, A., Murray, S. M. & Sourjik, V. A System for Gene Expression Noise Control in Yeast. *ACS Synth. Biol.* **7**, 2618–2626 (2018).

30. Pedone, E. *et al.* A tunable dual-input system for on-demand dynamic gene expression regulation. *Nat. Commun.* **10**, 4481 (2019).

31. Michaels, Y. S. *et al.* Precise tuning of gene expression levels in mammalian cells. *Nat. Commun.* **10**, 818 (2019).

32. Aranda-Díaz, A., Mace, K., Zuleta, I., Harrigan, P. & El-Samad, H. Robust Synthetic Circuits for Two-Dimensional Control of Gene Expression in Yeast. *ACS Synth. Biol.* **6**, 545–554 (2017).

33. Gao, Y. *et al.* Complex transcriptional modulation with orthogonal and inducible dCas9 regulators. *Nat. Methods* **13**, 1043–1049 (2016).

34. Liang, F.-S., Ho, W. Q. & Crabtree, G. R. Engineering the ABA plant stress pathway for regulation of induced proximity. *Sci. Signal.* **4**, rs2 (2011).

35. Miyamoto, T. *et al.* Rapid and orthogonal logic gating with a gibberellin-induced dimerization system. *Nat. Chem. Biol.* **8**, 465–470 (2012).

36. Baim, S. B., Labow, M. A., Levine, A. J. & Shenk, T. A chimeric mammalian transactivator based on the lac repressor that is regulated by temperature and isopropyl beta-D-thiogalactopyranoside. *Proc. Natl. Acad. Sci. U. S. A.* **88**, 5072–5076 (1991).

37. Chen, Y. *et al.* Tuning the dynamic range of bacterial promoters regulated by ligand-inducible transcription factors. *Nat. Commun.* **9**, 64 (2018).

38. Louvion, J. F., Havaux-Copf, B. & Picard, D. Fusion of GAL4-VP16 to a steroid-binding domain provides a tool for gratuitous induction of galactose-responsive genes in yeast. *Gene* **131**, 129–134 (1993).

39. Gossen, M. & Bujard, H. Tight control of gene expression in mammalian cells by

tetracycline-responsive promoters. *Proc. Natl. Acad. Sci. U. S. A.* **89**, 5547–5551 (1992).

40. Gossen, M. *et al.* Transcriptional activation by tetracyclines in mammalian cells. *Science* vol. 268 1766–1769 (1995).
41. Swain, P. S., Elowitz, M. B. & Siggia, E. D. Intrinsic and extrinsic contributions to stochasticity in gene expression. *Proc. Natl. Acad. Sci. U. S. A.* **99**, 12795–12800 (2002).
42. Müller, A. *et al.* Involvement of chemokine receptors in breast cancer metastasis. *Nature* vol. 410 50–56 (2001).
43. Liang, T., Wang, B., Li, J. & Liu, Y. LINC00922 Accelerates the Proliferation, Migration and Invasion of Lung Cancer Via the miRNA-204/CXCR4 Axis. *Med. Sci. Monit.* **25**, 5075–5086 (2019).
44. Horlbeck, M. A. *et al.* Compact and highly active next-generation libraries for CRISPR-mediated gene repression and activation. *Elife* **5**, (2016).
45. Zalatan, J. G. *et al.* Engineering complex synthetic transcriptional programs with CRISPR RNA scaffolds. *Cell* **160**, 339–350 (2015).
46. Tanenbaum, M. E., Gilbert, L. A., Qi, L. S., Weissman, J. S. & Vale, R. D. A protein-tagging system for signal amplification in gene expression and fluorescence imaging. *Cell* **159**, 635–646 (2014).
47. Fonseca, J. P. *et al.* A Toolkit for Rapid Modular Construction of Biological Circuits in Mammalian Cells. *ACS Synth. Biol.* **8**, 2593–2606 (2019).
48. Fonseca, J., Bonny, A., Town, J. & El-Samad, H. Assembly of Genetic Circuits with the Mammalian ToolKit. *BIO-PROTOCOL* vol. 10 (2020).

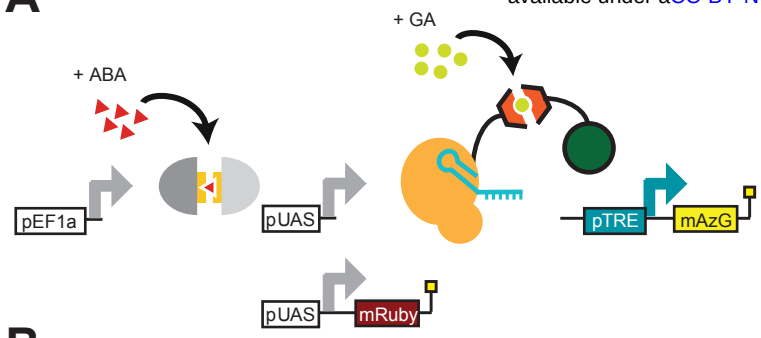

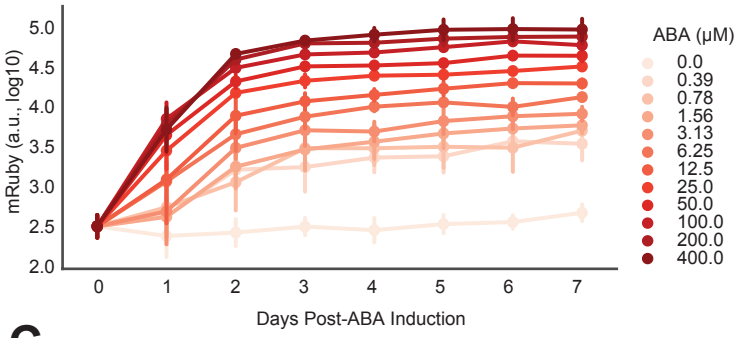

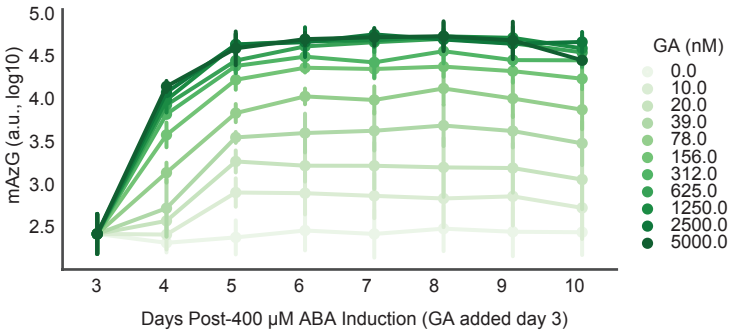

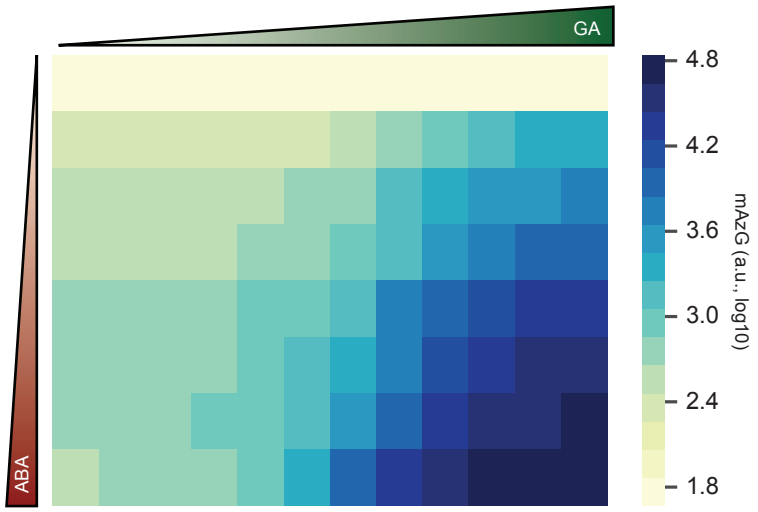

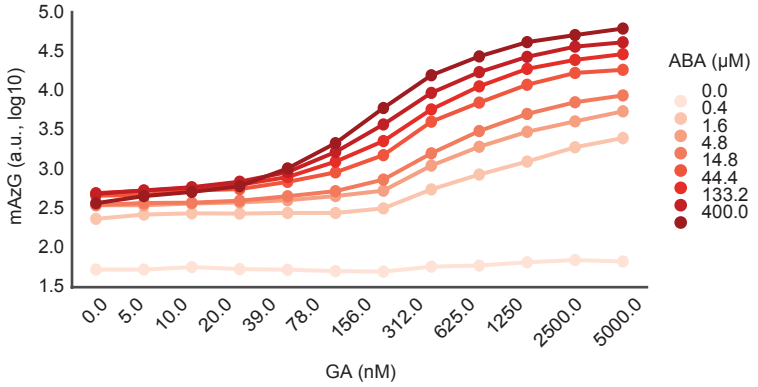

Figure 1

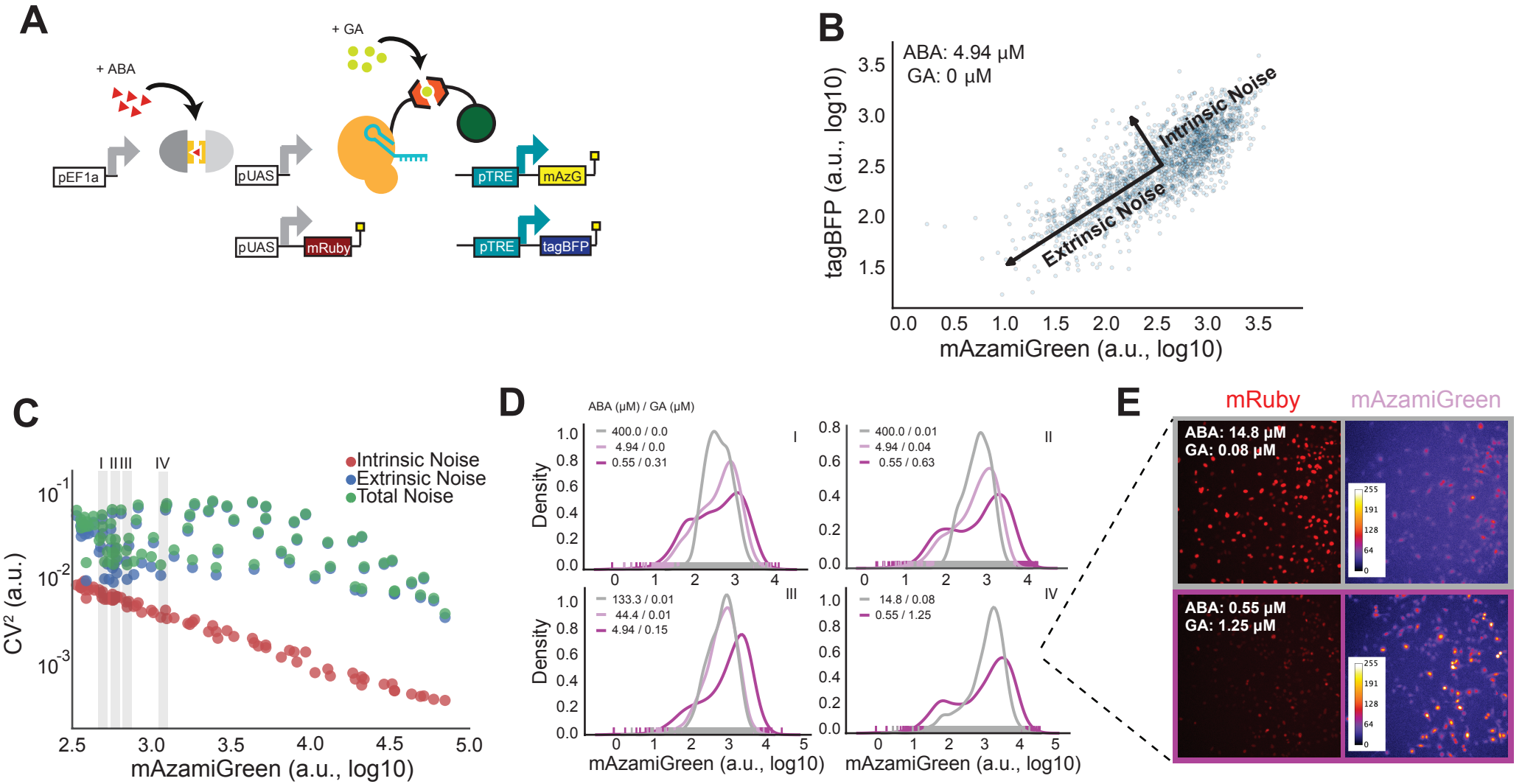
A
+ ABA
+ GA
pEF1a
pUAS
pUAS
mRuby
pTRE
mAzG
pTRE
tagBFP
B
ABA: 4.94 µM
GA: 0 µM
Intrinsic Noise
Extrinsic Noise
tagBFP (a.u., log10)
mAzamiGreen (a.u., log10)
C
I II III IV
Intrinsic Noise
Extrinsic Noise
Total Noise
CV² (a.u.)
mAzamiGreen (a.u., log10)
D
ABA (µM) / GA (µM)
400.0 / 0.0
4.94 / 0.0
0.55 / 0.31
400.0 / 0.01
4.94 / 0.04
0.55 / 0.63
133.3 / 0.01
44.4 / 0.01
4.94 / 0.15
14.8 / 0.08
0.55 / 1.25
Density
mAzamiGreen (a.u., log10)
E
mRuby
mAzamiGreen
ABA: 14.8 µM
GA: 0.08 µM
ABA: 0.55 µM
GA: 1.25 µM

Figure 2

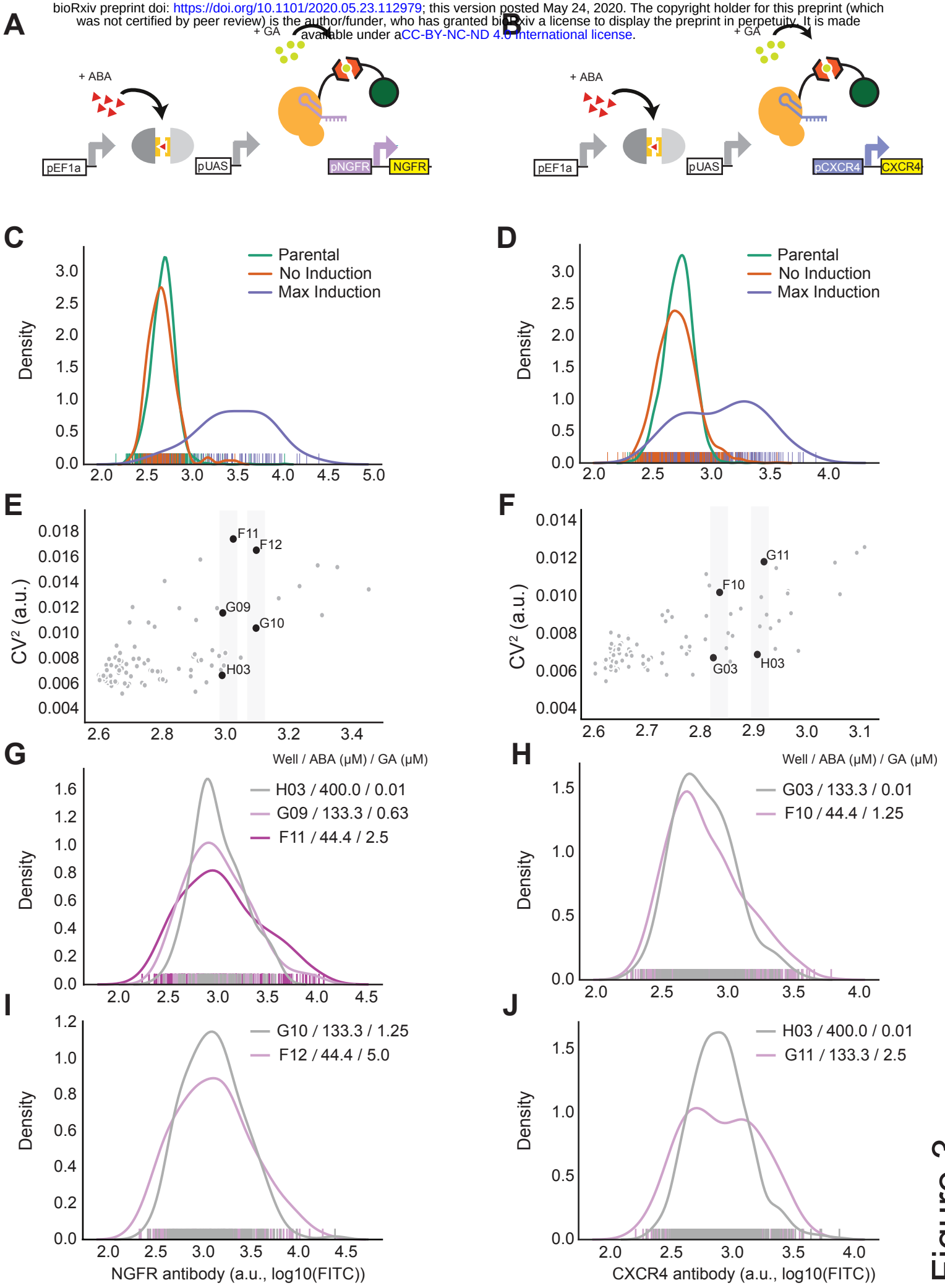

Figure 3